*Pol. J. Environ. Stud. Vol. 34, No. 6 (2025), 7287-7297*
DOI: *10.15244/pjoes/193143* ONLINE PUBLICATION DATE: 2024-11-08

*Original Research*

# Agglomeration and Removal of Submicron Fine Particulate Matter as a Result of Acidification and Evaporation

**Yu Niu[1], Yingying Xiong[1]*, Xian Niu[2, 3], Yuqi Wang[1], Zhiqian Wang[1], Feifang Wang[1]**

[1]Address School of Electric Power, Civil Engineering and Architecture, Shanxi University, Taiyuan, 030006, P.R. China
[2]School of Mining and Technology, Inner Mongolia University of Technology, Hohhot 010051, P.R. China
[3]Key lab. of University of Geological Hazards and Geotechnical Engineering Defense in Sandy, Drought and Cold Regions, Inner Mongolia Autonomous Region, Hohhot 010051, P.R. China

*Received: 6 June 2024*
*Accepted: 9 September 2024*

## Abstract

This study investigates the efficacy of coal dust removal using a wet-acid-ash experimental platform that incorporates flue-temperature coupling. The acidification–evaporation method was employed to quantify the dust eliminated from the flue gas and examine the particle-size distribution of submicron particles before and after the dust-removal process. These measurements were conducted under various conditions, including acidification, coupled humidification, cooling, and particle-concentration variations. Based on these experimental findings, we examined the aggregation and removal behaviors of submicron fine particulate matter. The temperature of the simulated hot dust-laden flue gas decreased from 120°C to 80°C, while the absolute humidity was adjusted to 8.90%, acidity to 4.183 ppm, and fly-ash particle concentration to 385.27 μg·m. Notably, there was a significant increase in the mean diameter of the volume distribution of submicron fine particles undergoing agglomeration, rising from to 20–37μm to 51.355μm. After the dust-removal procedure, the effectiveness of the dust collector reached 99.63%, thereby successfully removing submicron fine particles. Furthermore, the mean diameter of the number distribution decreased from 1.769 to 0.869 μm. The experimental results demonstrate that when flue gas is evaporated through a high temperature and coupled with humidity and acid ash, the ability of fly ash particles to adsorb aerosol droplets is enhanced. This enhancement promotes mutual adhesion among the submicron fine particles, intensifying their agglomeration. Consequently, the agglomerated particles are effectively captured by the dust collector, facilitating the removal and reduction of submicron fine particles.

**Keywords:** acidification evaporation, agglomeration, removal, submicron fine particulate matter, air pollution control

*e-mail: xiongyy@sxu.edu.cn

## Introduction

Coal-fired power plants (CFPPs) are significant sources of particulate emissions in China. The fumes produced by these plants contain environmentally hazardous substances, such as condensable particulate matter (CPM) and filterable particulate matter (FPM), which pose ecological dangers [1, 2]. CPM is a major contributor to particulate matter (PM), accounting for 55.9%–95.1% of the total, and its emissions are much higher than those of FPM [3, 4]. CPM condenses rapidly from a gaseous to a liquid or solid state at high flue temperatures, with organic components dominating, particularly saturated hydrocarbons (49.19–67.47%) and four-ring carcinogenic polycyclic aromatic hydrocarbons (C-PAHs) (almost 80%) [5]. However, 77.64% of the CPM released by Yantai City's CFPPs was composed of inorganic species, with $SO_4^{2-}$ having the highest concentration (23.74%), followed by Cl (11.95%). Moreover, 22.36% was organic matter, with alkanes comprising the majority of the organic fraction (72.7%) [6].

The release of PM, particularly $PM_{2.5}$, is a significant concern because of its adverse effects on the environment and potential health risks [7]. The organic fraction accounts for half of the CPM measured at the outlets of the low-low-temperature electrostatic precipitator (LLT-ESP), wet flue-gas desulfurization (WFGD), and wet electrostatic precipitator (WESP) [8]. Existing dust-removal technologies, such as static vacuum cleaners (electrostatic precipitators, ESP) and bag-like vacuum removers, can remove up to 99% of large particles measuring more than 2.5 microns in diameter [9]. The FPM and CPM concentrations in ultra-low emission coal-fired units vary from 0.81 to 7.52 mg/m³ and 1.10 to 12.25 mg/m³, respectively, depending on pollution control measures. Inorganic ions in CPM range from 1104 to 8240 μg/m³, with the majority being $SO_4^{2-}$ and $Ca^{2+}$ [10]. This emphasizes the need for emission control, including fuel treatment and optimization methods (such as fuel conversion, catalyst utilization, fuel lacquering, fuel additives, carbon-chain changes, gasification, and desulfurization) and equipment-modification methods, such as chimney and boiler modification [2, 11-14].

CPM can exist in solid, liquid, or semi-solid forms and is primarily found as droplets or spheres, with some heavy elements detected [4]. CPM is classified as $PM_{10}$ (diameter less than or equal to 10 microns) or $PM_{2.5}$ (diameter less than or equal to 2.5 microns) based on the particle size. $PM_{2.5}$ and $PM_{10}$ are two categories of PM, with the former having a finer size and a greater impact on human health. CPM is 10–30 times more prevalent in stack gas than filterable particulate matter ($FPM_{2.5}$) [15]. Common CPM removal procedures include filtering, wet dedusting, mechanical dedusting (inertial separation), electrostatic precipitation (electrostatic force), and wet flue-gas desulfurization. Selection is based on particle size and operating circumstances, which can be applied before, during, or after combustion.

The Shanghai Comprehensive Emission Standards for Air Pollution stipulate that the maximum permitted emission concentration of sulfuric-acid mist is 5 mg/m³, and the maximum permitted emission rate is 1.1 kg/h. Although China has conducted numerous studies on CPM removal, coal-fired power plants have only achieved ultralow emissions of conventional pollutants. The emission of CPM formed by the condensation of $H_2SO_4$, $NH_3$, volatile organic compounds (VOCs), and other components has become increasingly prominent [16-18], and existing coal-fired flue-gas particulate-matter control technologies are mostly targeted at $FPM_{2.5}$. The majority of available data indicates that the primary component of CPM emissions from stationary sources is the inorganic fraction, and sulfate ions significantly contribute to this fraction [1]. Most control technologies are specifically designed to target filterable particles, and a select few studies have delved into integrating various treatment techniques to encourage the aggregation and subsequent elimination of submicron particles effectively. Cheng et al. conducted experiments in laboratory facilities equipped with coal-fired boilers, selective catalytic-reduction devices, static vacuum cleaners, and humid smoke-gas desulfurizers to study the effects of selective catalyst restoration (SCR) on particulate emission properties [19].

Flue-gas desulfurization (FGD) systems installed with dry and semi-dry systems and ammonia-based NOx control systems (AFC) emit less filterable particulate matter (FPM) but significantly more condensable particulate matter (CPM) than household stoves and low-capacity boilers [5]. As a result, the potential benefits of dissolving and absorbing gypsum slurries to reduce CPM emissions are suggested [20]. Yao investigated the particulate characteristics of three coal-fired heat boilers in northern China in front of wet flue-gas desulfurization (WFGD). However, WFGD is a complex system involving mass transfers and chemical reactions, and the removal efficiency of PM was 30.06%-74.26% [21, 22]. Sulfur dioxide was mainly removed by gas-solid reactions using wet sorbents [23]. The results indicated that the particulate-matter removal efficiencies of wet and semi-dry FGD systems were 29.44% and 22.28%, respectively. The size distributions of the PM were within the range of 0.7 to 4.7 μm in the inlet-flue gases of both FGDs [24].

CPM volume and particle size can grow considerably. CPM consists mostly of inorganic components such as sulfates, nitrates, nitrites, and heavy metals, with organic matter comprising 30-60%. In these plants, submicron particles interact via Brownian diffusion, humidification, collisions, and nucleation to form PM. This causes particle development and condensation [5]. Coalescence is affected by temperature, humidity, turbulence, and particle concentration. Pretreatment fusion technologies improve PM removal. Further research could investigate how temperature affects particle aggregation in order to increase removal efficiency. Chemical condensers can amplify and bridge airborne particles; however, their

performance is restricted for aerosols ranging between 0-1 μm. To enhance collision frequency, electrical, acoustic, and helium flow fields are proposed for aerosol-particle clusters. Static fusion is highly efficient for submicron aerosols. Electrically conveyed particles traverse an oscillating electric field, causing them to oscillate and collide with opposing charges, leading to clustering [19].

The fine particulate matter in the FGD slurry and flue gas increase remarkably with the addition of agglomerates, particularly submicron particulate matter. This leads to a decrease in the percentage of fine particles (less than 10 μm) in the slurry, which rose from 31.11% to 22.61% [25]. The formation of submicron particles is primarily associated with three processes: ultrafine particle condensation, heterogeneous condensation, and intrinsic inorganic mineral fragmentation and precipitation [26].

The two primary processes leading to the development of ultramicron particles are the breaking and fusing of inorganic minerals and the collision and agglomeration of submicron particles [27]. The dissolution and absorption of gypsum slurries have a positive impact on CPM emissions [20]. Observations revealed that spherical particles were more prevalent in submicron particles than in ultramicron particles, suggesting a higher likelihood or greater suitability of the heterogeneous condensation of inorganic mineral vapors for agglomerating submicron particles [7, 28]. It is significantly more challenging to remove fine particles smaller than 1 μm than to remove larger particles [3, 22]. Coagulation–agglomeration growth refers to chemical or physical methods that promote the condensation of water vapor on the surface of particles, or interparticle collision and agglomeration to form larger particles. Specific methods include flue-gas humidification, acoustic agglomeration, chemical agglomeration, and electrical enhancement of coagulation. The population of condensable particles is significantly reduced as a result of the discharge, leading to the capture of their charges. This effect is more pronounced at higher output voltages.

Studies have provided valuable insights into the effects of various processes on the behavior of fine particles. While progress has been made in understanding the influence of oxidative evaporation on $PM_{2.5}$ fusion and removal, the detailed mechanisms of this process are not fully understood. On this basis, this study further elucidates the mechanism of the influence of temperature–wet–acid ash coupling on the agglomeration and elimination of submicron particles, and proposes an experimental scheme for controlling the concentration of submicron particles, which provides data support for the development of related industries.

## Materials and Methods

### CPM Formation Mechanism

It is crucial to investigate the removal of fine particulates from the atmosphere for a more comprehensive analysis [29]. The formation of these particles involves three primary processes: physical condensation, a chemical reaction, and nucleation. Physical condensation is a critical component in the formation of condensable particulate matter (CPM). During high-temperature combustion, a small fraction of the inorganic compounds in the coal vaporizes, setting the stage for CPM formation [5].

The mechanisms underlying the formation and growth of particulates differ significantly [17]. One process involves the selective condensation of inorganic vapor onto pre-existing particles, leading to an increase in particle size and the emergence of an inhomogeneous size distribution. This process can also trigger particle agglomeration, further enhancing their complexity and size [27]. Another mechanism involves the collision, condensation, and random binding of particles, ultimately resulting in the formation of particles with a uniform size distribution. Notably, the former lacks a distinct surface or core for condensation to occur, whereas the latter often exhibits an uneven size distribution, reflecting fundamentally different processes in the production and evolution of CPM.

The formation of PM is greatly influenced by chemical processes. Salt formed from acids produced by combustion is a key component of PM [30]. Nucleation is another crucial process that occurs during both the partial and complete combustion of coal. Elements such as carbon, hydrogen, and oxygen undergo transformations, leading to the formation of minute particles within the flue gas. As smoke gas cools, typically below 200°C, sulfur trioxide and water vapor unite to form sulfuric acid, further contributing to the formation of PM [31].

Various processes aid the formation of PM. A decrease in the condensation temperature increases the concentrations of nitrate and nitrite ions, which adds complexity to the particulate-matter formation process. Additionally, the presence of water vapor exacerbates this situation, further promoting the formation of these ions.

An in-depth study comparing CPM emissions from burning coal, pine, and sewage sludge revealed noteworthy patterns. Sewage sludge generated the highest concentration of CPM (19.79 $mg/m^3$), followed by coal (14.1 $mg/m^3$) and pine (7.57 $mg/m^3$) [32]. Scholars worldwide have compiled data on TPM concentrations and CPM components from various combustion sources [17]. This is because they have different ingredients. This may be another strategy to reduce CPM emissions.

*Mechanical Forces and Models*

Particles are drawn to one another and bind together under a variety of forces in a process known as agglomeration–coagulation, which is a crucial step in the formation of condensable particle matter. Several forces, including electrostatic, Brownian, van der Waals, and thermophoretic, are primarily applied to the PM during this process. The interaction force resulting from the charged surface of PM is known as the electrostatic force. Agglomeration is encouraged in high-temperature and high-humidity environments because friction and contact can charge PM. This leads to electrostatic attraction between the particles. The electrostatic force between two point charges can be expressed as follows [33, 34]:

$$F_1 = k\frac{Q_1 Q_2}{d^2}$$

Subsequently, when PM is exposed to the thermal motion of molecules in a fluid, a random force known as the Brownian force is created. This force increases the likelihood of inter-particle collisions, which in turn encourages agglomeration by causing the PM to move irregularly in space perpetually, can be expressed by the following equation:

$$F_2 = 6\pi\eta r^2 v\frac{r^2}{d^2}$$

Furthermore, every molecule is subject to the van der Waals force, an intermolecular force. The agglomeration process of sub-micron fine particles is significantly influenced by van der Waals forces because of their large specific surface area and surface energy.

$$F_3 = \mathrm{A}(d^3 - d^2)$$

The particles are drawn to one another and firmly bind together as a result of this mutual attraction. The force of particle movement is thermophoresis.

$$F_4 = -\mathrm{b}\frac{\mathrm{d}T}{\mathrm{dx}}\frac{r^2}{d^2}$$

Where $F_1$is the electrostatic force, $F_2$ is the Brownian force, $F_3$ is the van der Waals forces, $F_4$ is the thermophoresis, $k$ is the Coulomb constant, $Q_1$ and $Q_2$ are the electric quantities of the two-point charges, and $d$ is the distance between them, $r$ is the particle radius, $\eta$ is the fluid viscosity, $v$ is the particle velocity, b is a constant and d$T$/dx is the temperature gradient.

A flue gas moisture content-temperature diagram, which illustrates how water vapor condenses and releases latent heat as the flue gas temperature falls below the dew point, effectively analyzes the cooling process. The phase change features are reflected in the graph representation of this process, which is a state point traveling along a certain curve. The temperature, moisture content, and phase shift of the flue gas throughout the cooling process may all be determined by analyzing the trajectory. The flue gas cooling process was analyzed using the flue gas moisture content-temperature diagram. According to the definition of humidity content, the humidity content of flue gas is [35]:

$$\omega_{\mathrm{fg}} = \frac{q_{\mathrm{fgv}}}{q_{\mathrm{dfg}}} = \frac{n_{\mathrm{fgv}}\,M_{\mathrm{v}}}{n_{\mathrm{dfg}}\,M_{\mathrm{dfg}}}$$

According to Dalton's partial pressure law and the definition of relative humidity, the humidity content of the flue gas can be expressed as:

$$\omega_{\mathrm{fg}} = \frac{n_{\mathrm{fgv}}\,M_{\mathrm{v}}}{n_{\mathrm{dfg}}\,M_{\mathrm{dfg}}} = \frac{M_{\mathrm{v}}}{M_{\mathrm{dfg}}}\,\frac{\varphi_{\mathrm{fgv}}\,p_{\mathrm{fgs}}(t)}{p_{\mathrm{fg}} - \varphi_{\mathrm{fgv}}\,p_{\mathrm{fgs}}(t)}$$

And the humidity content of the air can be expressed as:

$$\omega_{\mathrm{a}} = \frac{n_{\mathrm{fgv}}\,M_{\mathrm{av}}}{n_{\mathrm{dfg}}\,M_{\mathrm{da}}} = \frac{M_{\mathrm{av}}}{M_{\mathrm{da}}}\,\frac{\varphi_{\mathrm{av}}\,p_{\mathrm{as}}(t)}{p_{\mathrm{a}} - \varphi_{\mathrm{av}}\,p_{\mathrm{as}}(t)}$$

The relationship between the water vapor pressure $p_{as}$ and its temperature $T$ is given by the Goff-Gratch equation:

$$\begin{cases} \lg p_{\mathrm{as}} = -7.9\left(\dfrac{373.16}{T} - 1\right) + 5.02\lg\left(\dfrac{373.16}{T}\right) \\ \quad - 1.38\times10^{-7}\left(10^{11.34\left(1-\frac{373.16}{T}\right)} - 1\right) \\ \quad + 8.13\times10^{-3}\left(10^{-3.49\left(\frac{373.16}{T}-1\right)} - 1\right) \\ \quad + \lg 1013.25 \qquad T > 273.15\ \mathrm{K} \\ \\ \lg p_{\mathrm{as}} = -9.1\left(\dfrac{373.16}{T} - 1\right) - 3.57\lg\left(\dfrac{373.16}{T}\right) \\ + 0.88\left(1 - \dfrac{373.16}{T}\right) + \lg 6.11 \quad T \le 273.15\ \mathrm{K} \end{cases}$$

where $\omega_{\mathrm{fg}}$ and $\omega_{\mathrm{a}}$ are, respectively, the moisture contents of flue gas and air, *g*/*kg*; $q_{\mathrm{fgv}}$ and $q_{\mathrm{dfg}}$ are, respectively, the wet flue-gas and dry flue-gas mass flows, *kg*/*s*; $n_{\mathrm{fgv}}$ and $n_{\mathrm{dfg}}$ are the amounts of material in the wet flue gas, and dry flue gas, *mol*; $M_{\mathrm{fgv}}$ and $M_{\mathrm{dfg}}$ are the molecular weight of the wet flue gas and dry flue gas, *kg*/*mol;* $p_{\mathrm{fgs}}$ and $p_{\mathrm{fg}}$ correspond to the temperature of the saturation pressure and smoke pressure of the wet flue gas, Pa; $\varphi_{\mathrm{fgv}}$ is the relative humidity of the flue gas, %; $T$ is the flue-gas temperature,°C; $M_{\mathrm{av}}$ and $M_{\mathrm{da}}$ are the molecular masses of water vapor and dry air, *kg*/*mol*,

respectively; $p_{as}$ and $p_a$ are the saturation pressure of wet air at the corresponding temperature and the pressure of dry air, Pa; and $\varphi_{av}$ is the relative humidity of the air, %.

### *Influence Factors*

CPM submicron fine PM forms and aggregates for various reasons. The inherent features of PM, namely its size distribution and chemical makeup, play a crucial role in determining the efficiency of the agglomeration and conversion rate in the atmosphere. Temperature, humidity, and pressure are examples of environmental elements that indirectly influence the agglomeration process by influencing the physical conditions and pace of the chemical reactions of the particles [1, 7, 29]. Additionally, kinetic characteristics, such as airflow direction and speed, turbulence intensity, etc., further affect the agglomeration effect by changing the trajectory and frequency of particle collisions [36].

In summary, a comprehensive understanding of the formation and consolidation processes of CPM submicron fine PM requires a detailed examination of the combined impact of its intrinsic characteristics and external environmental factors. By precisely controlling these factors, we can successfully manage the agglomeration process of PM and establish a scientific foundation for environmental preservation and enhanced air quality.

## Testing Facilities

This theme group presents a new idea and method of CPM cold-electrode field capture based on multi-field cooperation. By modifying the structure and operation of the dust-removal system, we conducted a wet-acid-ash coupling test bench and flue-gas temperature, as shown in Fig. 1. We simultaneously used multifaceted coagulation synergies in one device to promote condensation, reunification, and capture.

As shown in Fig. 1, there is a lot of equipment present in the test stand:

The flue gas configuration device is used to simulate the configuration of the flue gas in the section for composition. After the configuration is completed, the flue gas temperature can be instantly controlled and adjusted by the measurement and control system. The flue gas wet-acid-ash coupling device is used to simulate the natural coupling of the configured flue gas. Heat exchanger device is used for hot flue gas in the duct through the tube type cast iron heat exchanger and cooling water countercurrent contact, cooling water through the frequency conversion water pump regulation. An acid dewpoint test device unit is used to determine the condensation temperature of the sulfuric acid vapor in the flue gas. The electrostatic precipitator used is a horizontal electrostatic precipitator with adjustable voltage; the interior of the precipitator is equipped with two sets of parallel-arranged airflow distribution plates, and the discharge electrodes are made of pin-pricked high-strength nickel-cadmium alloy. The recirculation unit is used to recirculate the flue gases at a constant air velocity. A fan is used to drive the flue gas flow. A three-way valve is used to control the direction of flue gas flow.

There are two ways to circulate the test bench: firstly, the configuration of the flue gas is cooled down and then circulated at a certain flow rate through the recirculation section; secondly, the configuration of the flue gas is cooled down and then de-dusted through an electric precipitator. The flue gases passing through the fan can be circulated through a three-way valve or discharged through a chimney.

The Testo 350Pro flue-gas analyzer was used to test the simulated flue-gas composition and volume fraction, as shown in Fig. 2. The absolute humidity was measured and monitored in real-time using a Model 545 flue-gas moisture and humidity meter and controlled by the atomizing nozzle device in the conditioning section. The

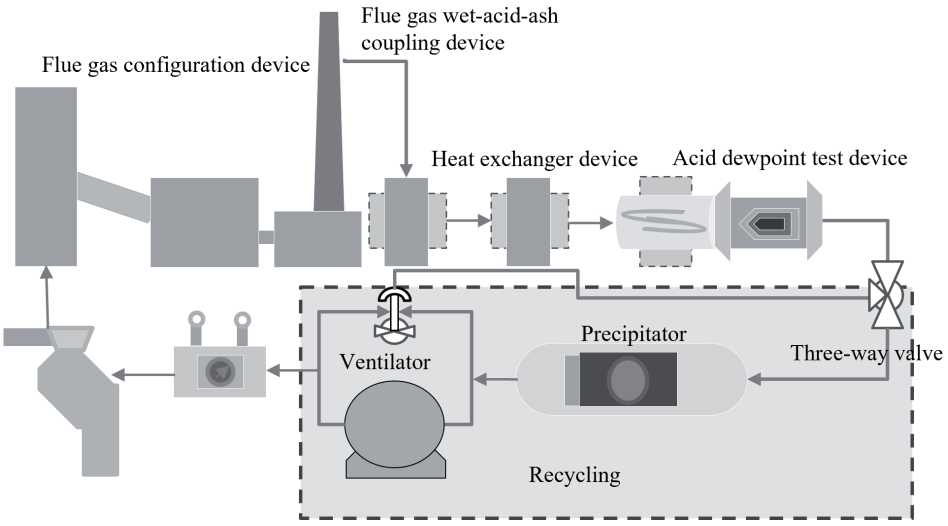


Fig. 1. Diagrammatic representation of the multi-pollutant synergistic removal experimental coal-fired flue gas CPM.

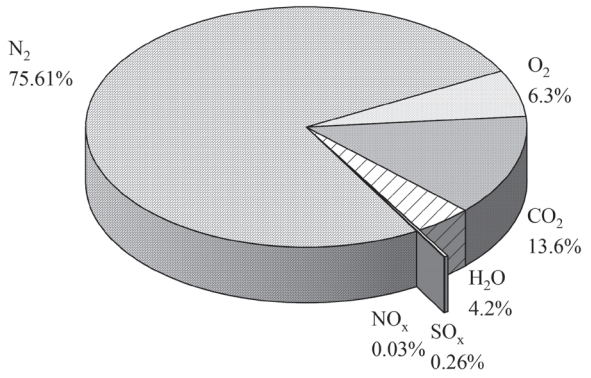


Fig. 2. Composition and volume of simulated flue gas.

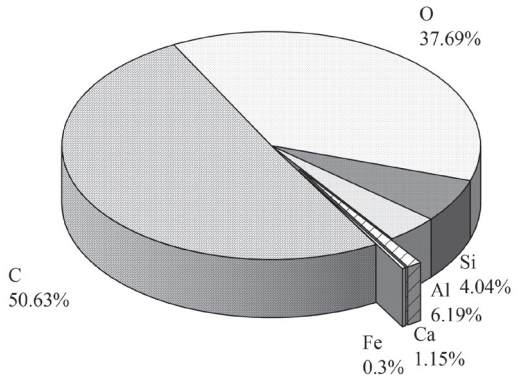


Fig. 3. Composition analysis of particulate matter.

flue-gas fly ash PM was concentrated by adjusting the rotational speed of the ZG600/YZ35-13 peristaltic pump. Laser $PM_{2.5}$ sensors were installed at the inlet and outlet of the dust collector. The particle size of submicron fine particles was measured by the Microtrac S3500 particle-size analyzer with a measuring range of 0.02–2800 μm.

### Main Parameter Determination and Performance Description

Considering the principle of higher removal efficiency and the convenience of dust collection, the main process parameters are as follows:

(1) The working voltage of the electrostatic precipitator is 40 kV, with a limited flow function. The flue gas in the precipitator remains at that speed for about 5 s; the airflow velocity is approximately 0.3 m/s, the diameters of the precipitator inlet and outlet pipeline are 200 mm, and the flow rate is approximately 0.03 $m^3/s$. The heat exchanger at the duct has a flow rate of about 4 m/s.

(2) The flue-gas temperature is less than 150°C; the humidity and acidity are regulated to ensure that the specific dust resistance is 104–1011 Ω·cm, suitable for the collection range of the electrostatic precipitator. The flue-gas temperature should be higher than 80°C to prevent the corona voltage from rising markedly, the voltage output of the electric field from being reduced, and the operation of the transformer being overloaded.

(3) The air duct is maintained at -0.69 kPa, which is convenient for flue-gas atomization, humidification, acidification, and particle-concentration adjustment.

(4) The acid dew point of each typical condition refers to the original flue-gas conditions of the engineering acid dew point. With the same conditions as the theoretical calculations [37, 38] (calculated using the acid dew-point expression of Russia, the former Soviet Union, and the Japanese Power Company) and considering the margin of error, the acid dew point was determined to be 83°C.

(5) A QUANTAX200 energy spectrometer was used to determine the composition of the PM, which consisted of silica–aluminum mineral particles and was moderately wettable, as shown in Fig. 3.

## Results and Discussion

### Effect of the Flue-Gas Temperature on the Aggregation and Removal Efficiency

Our setup simulated the flue-gas purification process of a coal-fired power plant. The temperature and velocity of the flue gas at the WFGD system inlet were set to 120°C and 3.5 m/s, respectively. When the peristaltic pump speed was 200 r/min, and the particle concentration was 72.362 $μg/m^3$, the inlet flue-gas temperature of the dust collector was reduced from the original 120°C working condition to 85°C (higher than the acid dew-point condition), 83°C (acid dew-point condition), and 80°C (limit condition). The influence of the flue-gas temperature on the agglomeration and removal performance is shown in Fig. 4.

As the dust-collector inlet flue-gas temperature decreased, the condensable gas in the flue gas condensed and was adsorbed by PM under the action of the van der Waals force. The concentration of PM at the dust-collector inlet gradually increased from 72.362 $μg/m^3$ to 92.362 $μg/m^3$, and the particles collided and were agglomerated under the drag force of the flue gas. The average particle size reflecting the number distribution increased from 1.769 μm before cooling to 2.090 μm. Then, the agglomeration effect of the submicron fine particles gradually appeared in the collision of continuous cooling, and the maximum agglomeration was 4.643 μm.

With the decrease of the flue-gas temperature at the dust-collector inlet, the thermal-motion ability of the flue gas is weakened, and the viscosity is reduced, while the heat released by the condensation of the flue gas generates thermophoretic force. As the flow field fluctuates slightly, the average particle size of the inlet-volume distribution is intensified by inertial collisions, and the particle size is aggregated from 20.370 μm before cooling to an easier-to-capture 31.391 μm.

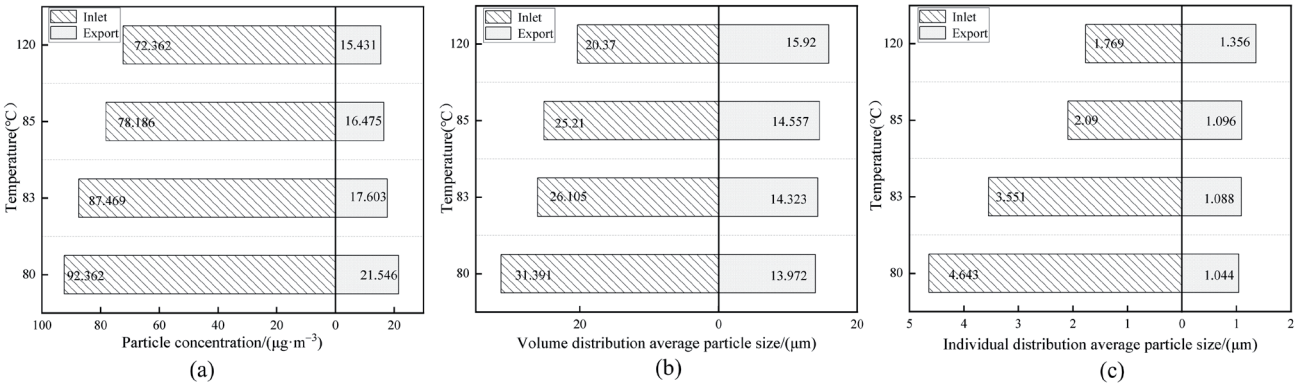


Fig. 4. The influence of flue gas temperature on agglomeration and removal performance matter.

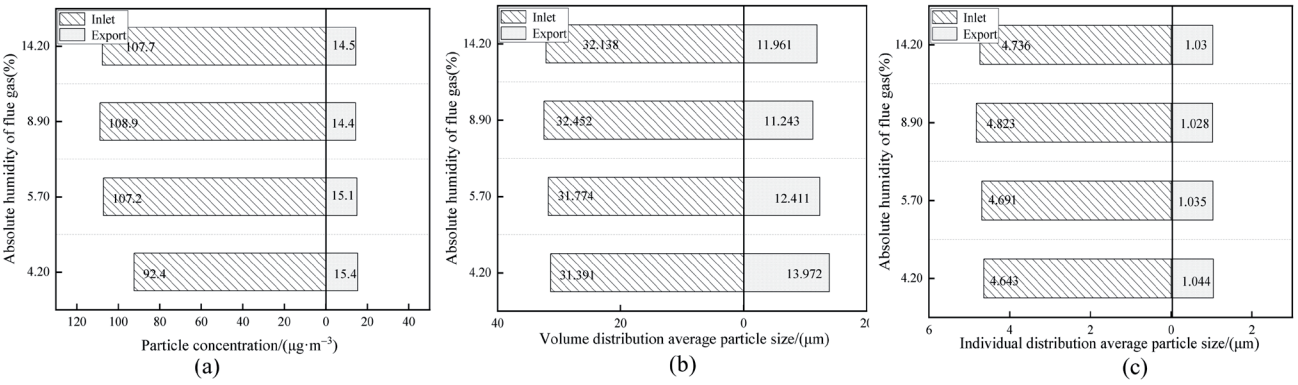


Fig. 5. The influence of flue gas absolute humidity on agglomeration and removal performance matter.

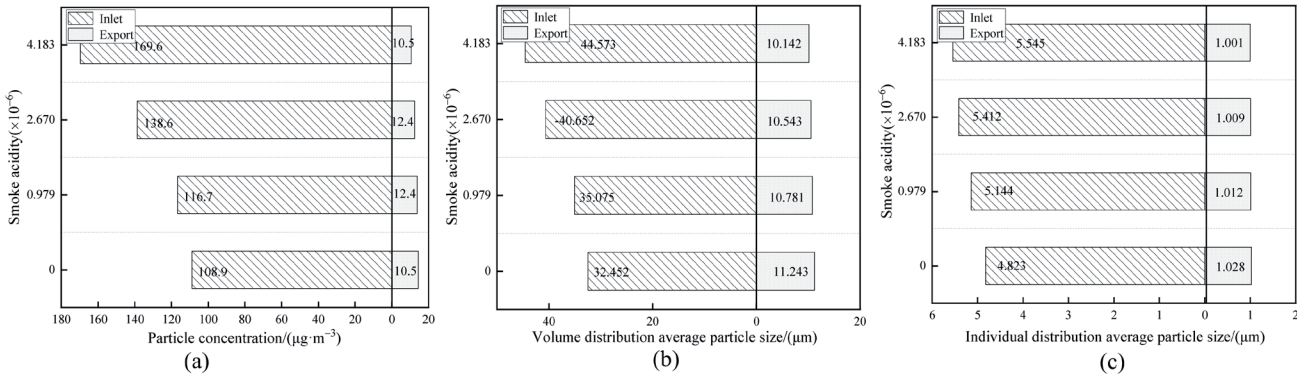


Fig. 6. The influence of flue gas acidity on agglomeration and removal performance matter.

Under an electric-field charge, the particle concentration at the precipitator outlet decreased from 21.546 μg/m$^3$ to a minimum of 15.431 μg/m$^3$ during the cooling process, and the dust-removal efficiency increased from 70.224% to 83.293%. After removal, the average particle size of the volume distribution decreased to 13.972 μm. The average particle size of the number distribution decreased to 1.044 μm, which was a 0.725-μm decrease compared with the original particle size before cooling. The removal effect was obvious.

Flue gas, initially at 4.20% humidity, was humidified during cooling from 120°C to 80°C, reaching 5.70%, 8.90%, and 14.20% humidity. Fig. 5 depicts how these humidity changes affected agglomeration and particle removal efficiency.

Fig.5 (a) depicts the relationship between particle concentration (in μg·m$^{-3}$) and the particle size distribution, with a focus on the inlet and export concentrations of particles within the 0-20 micrometer range. High water surface tension and medium-low

particle adhesion limited moisture absorption, resulting in increased inlet particle concentration up to 108.9 μg/m³ at 8.90% humidity, then slightly decreased to 107.7 μg/m³ at 14.20% due to saturation.

As shown in Fig.5 (b) and Fig.5 (c), although the turbulence of smoke flow and wet droplets promotes particle aggregation, the average particle size at the inlet of the dust collector increased from 31.391 μ m to 32.452 μ m, failing to form larger aggregates. The limited concentration of particles at the inlet of the dust collector resulted in limited effective collisions between particles. The mean particle size of the number distribution increased to 4.823 μm at 8.90% absolute humidity, but decreased to 4.736 μm when the absolute humidity increased to 14.20% due to the diffusion of water droplets. After removal, the average particle size of the volume distribution was 11.243 μm, and the average particle size of the number distribution was about 1.028 μm. Compared with that before humidification, the removal effect was not obvious.

## Effect of Temperature–Wet–Acid Coupling on the Aggregation and Removal Efficiency

Under typical conditions with the highest humidification and removal efficiencies, and an absolute humidity of 8.90%, sulfuric-acid solutions with volume fractions of 0.11%, 0.30%, and 0.47% were configured, and the flue-gas acidities were $0.979\times10^{-6}$, $2.670\times10^{-6}$, and $4.183\times10^{-6}$, respectively. The flue gas was reduced from 120°C to 80°C by acidizing evaporation through the atomizer, and the temperature, humidity, and acid were coupled. The influence of the flue-gas acidity on the agglomeration and removal performance is shown in Fig. 6.

After humidification, acidification, and cooling, the acidity of the flue gas gradually increases, and the particulate-matter concentration at the dust-collector inlet increases significantly, from 108.859 μg/m³ before acidification and adjustment to a maximum of 169.589 μg/m³. In other words, during the flue-gas condensation process after humidification and acidification, the acid fog entered the pores and cavities of the fly ash surface under the action of electrostatic and pore-field forces. An acidic liquid film formed on the surface of the particles and the acidic gas was continuously dissolved. This effectively reduced the surface tension of the liquid film, further improved the hygroscopic properties of the particles, and increased mutual adhesion.

When the particulate matter concentration increases significantly, chemical adsorption occurs between the metal and liquid film in the PM. An ingredient comparison of PM before and after the coupling of temperature, humidity, and acid is shown in Fig. 7. It can be seen that after the temperature, humidity, and acid coupling, the Ca and Fe components in the particles decrease while the conductive ions in the liquid film increase. This improves the charging capacity of the particles, increases the collision probability between particles and between particles and agglomerated droplets, and increases the average particle size of the number distribution of the dust-collector inlet to 5.545 μm.

With the increase of the acid fog concentration, acid fog droplets are more likely to form a liquid bridging force between submicron fine particles than wet-fog droplets, and dispersed particles in the form of spheroid accumulations before agglomeration are aggregated through "bridging". With the evaporation of the acid-mist droplets, the liquid bridging force is continuously transformed into a bridge-fastening force. The particles flocculate, the amount of adsorbed acid fog increases, and the agglomeration force is further improved to form large particles. Scanning electron microscope (SEM) images before and after the temperature, humidity, and acid coupling of the particles are shown in Fig. 8. The average particle size of the inlet-volume distribution of the precipitator gradually increased from 32.452 μm to 44.573 μm, which was easier for the precipitator to capture than before the acidification.

The enhancement of the acid-mist droplet and particle agglomeration performance improved the

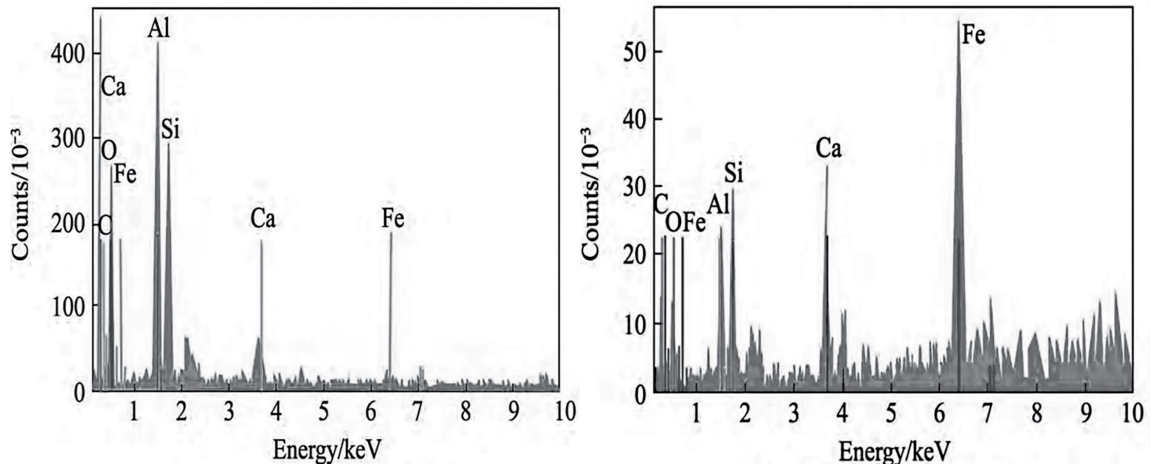


Fig. 7. Comparison of particulate matter composition before and after temp-humidity coupling.

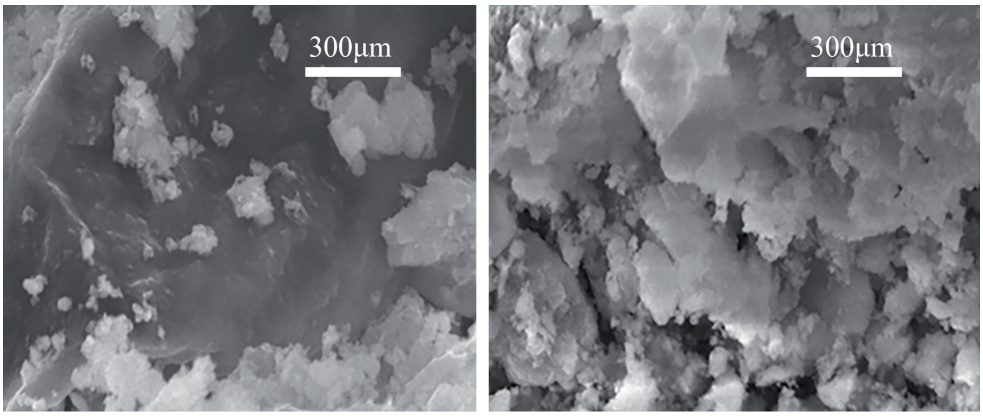


(a) Before coalescence (b) After coalescence

Fig. 8. The SEM image of particle scale before and after coalescence.

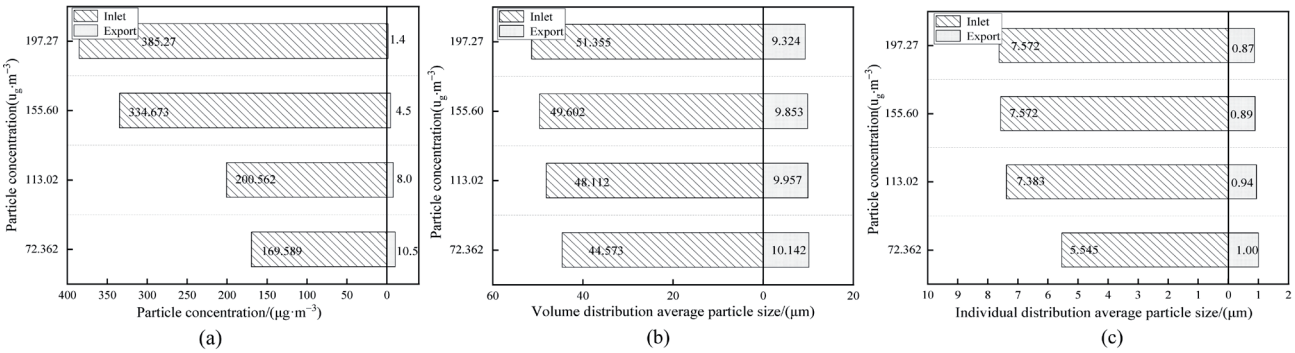


Fig. 9. The influence of particle concentration change on agglomeration and removal performance matter.

dust-collector removal performance. The particle concentration at the precipitator outlet decreased from 14.382 μg/m$^3$ to 10.511 μg/m$^3$. The dust-removal efficiency increased from 86.788% to 93.802%, and the average particle size of the volume distribution was 10.142 μm at the minimum. The average particle size of the number distribution was 1.001 μm, which decreased by 0.027 μm, compared with that before humidification, and the removal performance was significantly changed.

## Effect of the Temperature–Wet–Acid Ash Coupling on the Aggregation and Removal Efficiency

The flue-gas humidity was 8.90%. The coupled acidity was unchanged at $4.183\times10^{-6}$. The peristaltic pump speed was adjusted to 300, 400, and 500 r/min. The concentration of particles in the flue gas reached 113.02, 155.60, and 197.27 μg/m$^3$, respectively, and the flue gas cooled from 120°C to 80°C. The influence of the change in particle concentration on the agglomeration and removal performance is shown in Fig. 9.

When warm, wet, and acid ash were coupled, the particle concentration at the dust-collector inlet increased to 169.58, 200.562, and 334.673 μg/m$^3$, respectively, and the particle number increased accordingly. In addition, the radial distribution function in the duct and the contact between particles increased. Consequently, the collision probability between particles and the particle agglomeration under the coupling action of particles and warm, wet, and acid ash increased, and the turbulent effect of the flue-gas superposition resulted in intense turbulence and mixing. The average particle size of the precipitator inlet-number distribution rapidly increased from 5.545 μm to 7.572 μm, and the agglomeration obviously formed. The average particle size of the precipitator-inlet volume distribution also increased from 44.573 μm to 49.602 μm.

The concentration of PM at the precipitator inlet increased from 334.673 μg/m$^3$ to 385.270 μg/m$^3$. Under the action of inertia, the average amount of acid adsorbed on the surface of PM decreased, and the average particle size of the number and volume distributions of the precipitator inlet reached 7.624 and 51.355 μm, respectively, increasing by 0.052 and 1.753 μm, respectively. The coupled agglomerations of warm, wet, and acid ash were weakened.

During the process of gradually increasing the particle concentration, the agglomeration was efficiently captured by the dust collector. After removal, the particle concentration was reduced to 1.438 μg/m$^3$, and the removal efficiency reached 99.627%. The average particle sizes of the volume and number distributions

were 9.324 and 0.869 μm, respectively. The average particle size of the number distribution decreased by 0.132 μm compared with that before the coupling. Moreover, the characteristic parameters of PM at the dust-collector exit first increased and then decreased; that is, the removal effect was weakened when the concentration was too high.

## Conclusions

This study delves deeply into the changes in particle behavior that occur during the evaporation of temperature–wet–acid ash, with a particular emphasis on changes in particle affinity, unity, and static precipitator capture efficiency. Using novel experimental methodologies and research approaches, it was discovered that the evaporation process considerably improves particle affinity and unity, hence enhancing static precipitator capture efficiency.

Particle adhesion, condensation, and reaggregation are enhanced by the evaporation process as particle concentration rises. Particles are more likely to gravitate toward the inner diameter of the pipeline as a result of the increased collision frequency, which improves the effectiveness of static precipitators in capturing particles. However, the distribution of particle volumes gets more widely dispersed as the number of submicron particles grows, which, therefore, lowers the total aggregation efficiency.

A theoretical model for controlling submicron particle concentrations is proposed, offering a theoretical foundation for optimizing industrial processes and improving the dust removal effectiveness of static precipitators. By controlling particle concentrations in a way that maximizes affinity and unity, static precipitators can improve their capture efficiency. This not only aids in the reduction of environmental pollution but also encourages green production.

In conclusion, the temperature-wet-acid-ash coupling dust removal technology employed in this study has significantly reduced dust and greatly improved acidic emissions while eliminating particulate matter. In recent years, continuous improvements have been made to the emission standard and adjustments were introduced to the national flue gas emission policy. The temperature-wet-acid-ash coupling technology is in accordance with the trend of future policy development and has a promising future. Nevertheless, there are a few issues that have not been taken into account in this research, like the equipment's big footprint, complexity of operation, and potential harm from some byproducts created during the coupling process. In the following stage of the study, we will address these problems.

## Acknowledgments

This work was supported by the Shanxi Province Basic Research Program (Free Exploration) (202103021223031).

## Conflict of Interest

The authors declare no conflict of interest.

## References

1. WU D., ZHENG H., LI Q., JIN L., LYU R., DING X., HUO Y., ZHAO B., JIANG J., CHEN J., LI X., WANG S. Toxic potency-adjusted control of air pollution for solid fuel combustion. Nature Energy, **7** (2), 194, **2022**.
2. LARKI I., ZAHEDI A., ASADI M., FOROOTAN M.M., FARAJOLLAHI M., AHMADI R., AHMADI A. Mitigation approaches and techniques for combustion power plants flue gas emissions: A comprehensive review. Science of the Total Environment, **903**, 166108, **2023**.
3. YANG F.X., LI Z.H., LIU H.X., FENG P., TAN H.Z., ZHANG S.C., LU X.C. Emission characteristics of condensable particulate matter and sulfur trioxide from coal-fired power plants. Journal of the Energy Institute, **94**, 146, **2021**.
4. LIANG B., BAI H.L., TAN B., BAI D.R. Sources apportionment of water-soluble inorganic salts in CPM from coal-fired power plants with different emission control technologies. Fuel, **334**, 126786, **2023**.
5. WU Y.J., XU Z.Y., LIU S.Q., TANG M.H., LU S.Y. Emission of organic components and distribution characteristics of PAHs in condensable particulate matter from coal-fired power and industrial plants. Journal of the Energy Institute, **97**, 109, **2021**.
6. TONG H.H., WANG Y.J., TAO S.K., HUANG L., JIANG S., BIAN J.T., CHEN N., KASEMSAN M., YIN H.Y., HUANG C., CHEN H., ZHANG K., LI L. Developed compositional source profile and estimated emissions of condensable particulate matter from coal-fired power plants: A case study of Yantai, China. Science of the Total Environment, **869**, 161817, **2023**.
7. GUAN H.L., LIU Q.F., ZHANG C., WANG T., WANG J.W., WU G.Q., PAN W.P. Formation and migration of trace elements in condensable particulate matter with the finest particle size distribution. Journal of Hazardous Materials, **446**, 130750, **2023**.
8. SONG J.W., LU S.Y., WU Y.J., ZHOU C.Y., LI X.D., LI J.W. Migration and distribution characteristics of organic and inorganic fractions in condensable particulate matter emitted from an ultralow emission coal-fired power plant. Chemosphere, **243**, 125346, **2020**.
9. FENG Y.P., LI Y.Z., ZHANG X.Y., SU S.Q., ZHANG Z.P., GAN Z.W., DONG Y. Comparative study on the characteristics of condensable particulate matter emitted from three kinds of coal. Environmental Pollution, **270**, 116267, **2021**.
10. YANG Y.L., SU Q.F., ZHENG C.H., ZHANG Y., WANG Y.F., GUO D., HE Y.B., ZHU Y. Emission characteristics of filterable particulate matter and condensable particulate matter from coal-fired power plants. Case Studies in Thermal Engineering, **35**, 102145, **2022**.

11. WU B.B., BAI X.X., LIU W., LIN S.M., LIU S.H., LUO L.N., GUO Z.H., ZHAO S., LV Y.Q., ZHU C.Y., HAO Y., LIU Y., HAO J.M., DUAN L., TIAN H.Z. Non-Negligible Stack Emissions of Noncriteria Air Pollutants from Coal-Fired Power Plants in China: Condensable Particulate Matter and Sulfur Trioxide. Environmental Science & Technology, **54** (11), 6540, **2020**.
12. LIN X.H., YANG R.Q., ZHANG W., ZENG N., ZHAO Y., WANG G.C., LI T.T., CAI Q.X. An integrated view of correlated emissions of greenhouse gases and air pollutants in China. Carbon Balance and Management, **18** (1), 9, **2023**.
13. SUN C., LI B.J., CHEN L., GAO Y.C., JIN J.B., GU X., YANG Y., LOU Y.X., ZHAO Y.Q., LIAO H. An improved hourly-resolved atmospheric $NO_x$ emission inventory of industrial sources based on Continuous Emission Monitoring System data: Case of Jiangsu Province, China. Journal of Cleaner Production, **419**, 138192, **2023**.
14. TANG L., JIA M., YANG J.A., LI L., BO X., MI Z.F. Chinese industrial air pollution emissions based on the continuous emission monitoring systems network. Scientific Data, **10** (1), **2023**.
15. NGO T.H., YANG H.Y., PAN S.Y., CHANG M.B., CHI K.H. Condensable and filterable particulate matter emission of coal fired boilers and characteristics of PM2.5-bound polycyclic aromatic hydrocarbons in the vicinity. Fuel, **308**, 121833, **2022**.
16. WANG P., LIU D.C., MUKHERJEE A., AGRAWAL M., ZHANG H.W., AGATHOKLEOUS E., QIAO X., XU X.B., CHEN Y., WU T., ZHU M.Y., SAIKAWA E., AGRAWAL S.B., FENG Z.Z. Air pollution governance in China and India: Comparison and implications. Environmental Science & Policy, **142**, 112, **2023**.
17. LIU W.T., WANG X., ZHAO B.W., LU J.Y. New Insights into the Synergistic Effect on Condensable Particulate Matter Based on the Formation, Characteristics and Removal. Aerosol and Air Quality Research, **23** (12), 230145, **2023**.
18. YUAN C., WANG Z.W., CHENG H.R., CHEN J., LIANG S.W., SU S.Q., WANG P.C., ZHAN Y., JIANG L.X., XIONG Y. Assessing the impacts of CPM emitted from stationary sources on PM2.5 source appointment of Wuhan, China. Fuel, **337**, 126869, **2023**.
19. CHENG T., ZHENG C.Q., YANG L.J., WU H., FAN H.M. Effect of selective catalytic reduction denitrification on fine particulate matter emission characteristics. Fuel, **238** 18, **2019**.
20. LIANG B., BAI H.L., FU L.L., BAI D.R. Characteristics of the particulate matter and its toxic substances from different stationary coal-fired sources. Fuel, **334**, 126594, **2023**.
21. YAO S., CHENG S.Y., LI J.B., ZHANG H.Y., JIA J., SUN X.W. Effect of wet flue gas desulfurization (WFGD) on fine particle ($PM_{2.5}$) emission from coal-fired boilers. Journal of Environmental Sciences, **77**, 32, **2019**.
22. CHEN T.L., DENG L.J., LI Y.Z., LI J.W., ZHANG Z.P. Improvement of the reduction of condensable particulate matter in flue gas scrubbing process. Environmental Research, **237**, **2023**.
23. ZHENG C.H., WANG Y.F., LIU Y., YANG Z.D., QU R.Y., YE D., LIANG C.S., LIU S.J., GAO X. Formation, transformation, measurement, and control of $SO_3$ in coal-fired power plants. Fuel, **241**, 327, **2019**.
24. WANG H., ZHANG P. Emission characteristics of PM, heavy metals, and dioxins in flue gases from sintering machines with wet and semi-dry flue gas desulfurization systems. Environmental Science and Pollution Research, **28** (34), 46089, **2021**.
25. ZHOU L., LIU Y., LUO L.Y., YUAN Z.L., YANG L.J., WU H. Improving the removal of fine particles by chemical agglomeration during the limestone-gypsum wet flue gas desulfurization process. Journal of Environmental Sciences, **80**, 35, **2019**.
26. GE Z.F., CAO X., ZHA Z.T., MA Y.N., ZENG M.X., WU K., CHU S., TAO Y.J., ZHANG H.Y. The mineral transformation and molten behaviors of biomass waste ashes in gasification-melting process. Fuel Processing Technology, **226**, 107095, **2022**.
27. YUAN C., WANG Z.W., CHENG H.R., LIANG S.W., HU Y.Z., DONG X.Y., WU J.W. Characteristics of water-soluble ions in condensable particulate matter emitted from stationary sources in Wuhan. Fuel, **295**, 120626, **2021**.
28. SENIOR C., GRANITE E., LINAK W., SEAMES W. Chemistry of Trace Inorganic Elements in Coal Combustion Systems: A Century of Discovery. Energy & Fuels, **34** (12), 15141, **2020**.
29. LI J.W., LI X.D., WANG W.L., WANG X.J., LU S.Y., SUN J., MAO Y.P. Investigation on removal effects and condensation characteristics of condensable particulate matter: Field test and experimental study. Science of the Total Environment, **783**, 146985, **2021**.
30. KARPLUS V.J., WU M.Y. Dynamic responses of $SO_2$ pollution to China's environmental inspections. Proceedings of the National Academy of Sciences of the United States of America, **120** (17), **2023**.
31. ZHANG H.W., LI Y.Z., ZHANG Z.P., WANG L., RAN W.Z., CHEN T.L. Exploration on the source of $SO_4^{2-}$ in Condensable Particulate Matter. Fuel, **337**, 126949, **2023**.
32. ZHAI Y.F., LIU X.W., ZHANG A.Y., XU M.H. Comparison of the formation characteristics of condensable particulate matter from the combustion of three solid fuels. Fuel, **329**, 125492, **2022**.
33. SONG G.C., LI Y.X., WANG W.C., JIANG K., SHI Z.Z., YAO S.P. Numerical simulation of hydrate slurry flow behavior in oil-water systems based on hydrate agglomeration modelling. Journal of Petroleum Science and Engineering, **169**, 393, **2018**.
34. BREUER M., ALMOHAMMED N. Modeling and simulation of particle agglomeration in turbulent flows using a hard-sphere model with deterministic collision detection and enhanced structure models. International Journal of Multiphase Flow, **73**, 171, **2015**.
35. BAI T., JIN Z. Thermodynamic Analysis of Condensation Water and Waste Heat Recovery of Coal-fired Flue Gas. Journal of Chinese Society of Power Engineering, **42** (10), 977, **2022**.
36. SUN Z. Study on Promoting the Removal of Fine Particles and $SO_3$ in Coal-Fired Flue Gas by the Coupling of Turbulent and Chemical Agglomeration, Southeast University, **2021**.
37. YAO Q.P., LI R.Y., WANG Y.K., LI Y.H., ZHANG L., DENG L., CHE D.F. Feasibility Analysis of Coupling Hydrogen-Derived Fuel on a Coal- Fired Boiler for Power Generation. Energy & Fuels, **37** (1), 477, **2023**.
38. WEI W., SUN F.Z., SHI Y.T., MA L. Theoretical prediction of acid dew point and safe operating temperature of heat exchangers for coal-fired power plants. Applied Thermal Engineering, **123**, 782, **2017**.